

Ultrasonic Bending of Silver Nanowires

Qiuxian Chen, Wenwen Xin, Qiaozhen Ji, Ting Hu, Jun Zhang, Cheng Shang, Zhipan Liu, Xueyang Liu,* and Hongyu Chen*

Cite This: *ACS Nano* 2020, 14, 15286–15292

Read Online

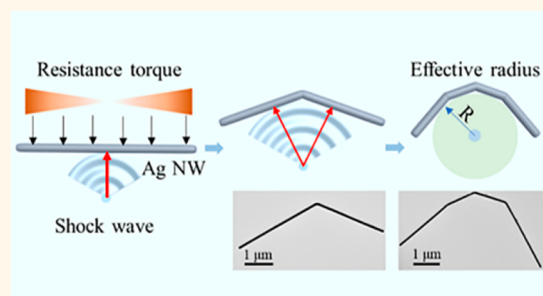
ACCESS |

Metrics & More

Article Recommendations

Supporting Information

ABSTRACT: We study silver nanowires as a model for the mechanical effects of ultrasonication. Their bending is caused by the outward push of shock waves against the inertia and fluid resistance. The structural analyses of a large number of cases reveal the principles of the mechanical effects on the freely suspended colloidal nanostructures. In addition to providing knowledge of the sonication effects, we believe that understanding would help to exploit sonication for nanoscale mechanical manipulation.



KEYWORDS: ultrasound, mechanical effect, silver nanowires, bending, cavitation

Ultrasonication is a sinusoidal sound wave with a frequency between 20 k and 1 GHz.¹ It has a wide range of applications in the chemical and biological fields,^{2–4} including cleaning reaction vessels, accelerating material dissolution, promoting chemical reactions, and cleaving DNA strands.^{5–7}

The main effect of ultrasound comes from cavitation: When the sound wave is in a negative pressure state, the liquid would be stretched and the solution is torn open to form a small cavity.⁸ The cavity grows rapidly under cyclic compression and stretching. Once reaching a limit, it would implode in a sub-microsecond time scale, generating a high temperature of 5000 °C and a high pressure of 1000 atm as a highly localized effect.^{1,9}

Ultrasonic cavitation has thermal and mechanical effects.¹⁰ The thermal effect refers to the spillover of the local high temperature, which can be used to promote chemical reactions, such as inducing reactive oxygen species.⁶ The mechanical effect refers to the broader effects of shear stress and shock waves, which can be used for emulsification, tissue cutting, and skin penetration.⁹

In the synthesis of nanomaterials, thermal effects have been typically used to promote chemical reactions,¹¹ for example, in the synthesis of molybdenum sulfide.^{12,13} In addition, mechanical effects have been widely used to disperse loose aggregates.^{14,15} In contrast, the morphological consequence of nanostructures has rarely been studied.

In this work, we study the mechanical effects of ultrasonication as a means of structural manipulation. Using pentagonal silver nanowires (Ag NWs) as the model, we find that the cavitation causes predictable bending and breaking of the Ag NWs. The consistent bending direction of multi-

segment structures suggests that the cavitation effects are interrelated, likely as part of a single event. The resulting half-circular shape reveals the effective radius of a shock wave. We believe that the fundamental understanding of the morphological consequences of sonication would expand the tools of manipulation and assist future effects in sophisticated nanosynthesis.

RESULTS AND DISCUSSION

Ultrasonic Bending of Ag NWs. The five-fold twinned Ag NWs¹⁶ were about 20 μm in length and 80 nm in diameter (Figure S1). The as-synthesized sample was washed with acetone to remove the remnant PVP, FeCl₃, and ethylene glycol. The isolated Ag NWs were dispersed in ethanol and then treated with ultrasonic cleaner at 250 W and 40 kHz for 1 h.

A random survey of the resulting Ag NWs showed that 88.7% of them were bent, forming two, three, or multiple segments (Figure 1B,D and Figure S6). The bending angles are often obtuse, and the multiple segments often bend towards the same direction (*vide infra*). The remaining 11.3% were straight with a relatively short length, suggesting that they have been broken. With the extension of ultrasonic time, the average total length of the Ag NWs became continuously shorter

Received: July 7, 2020

Accepted: November 9, 2020

Published: November 12, 2020



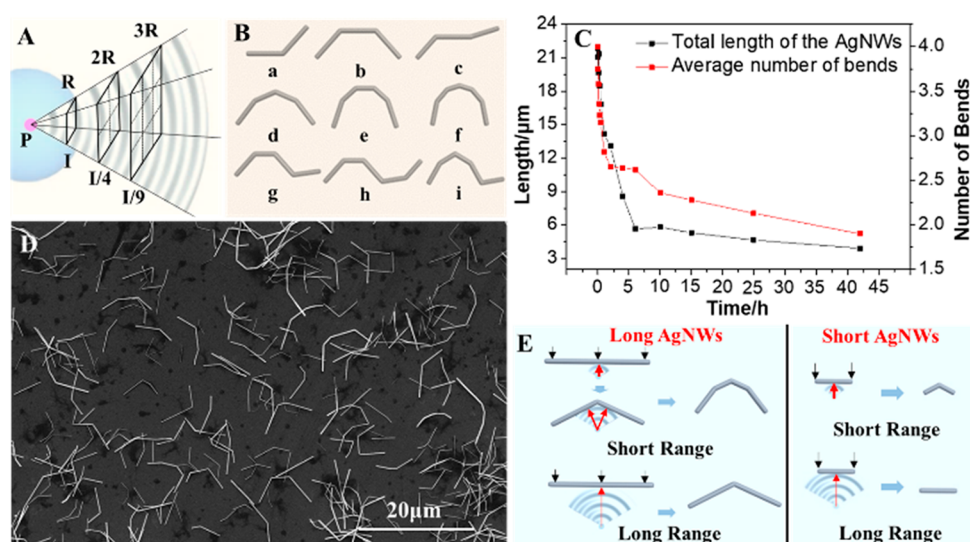


Figure 1. (A) Schematics representing the energy transmission for the shock wave after the collapse of ultrasonic cavity (P is the energy of the shock wave, and I is the energy density). (B) Bending patterns of the Ag NWs. (C) Temporal evolution of the total length and the average number of bends. (D) SEM image of the bent Ag NWs. (E) Bending diagram of long and short Ag NWs for long-range and short-range interactions.

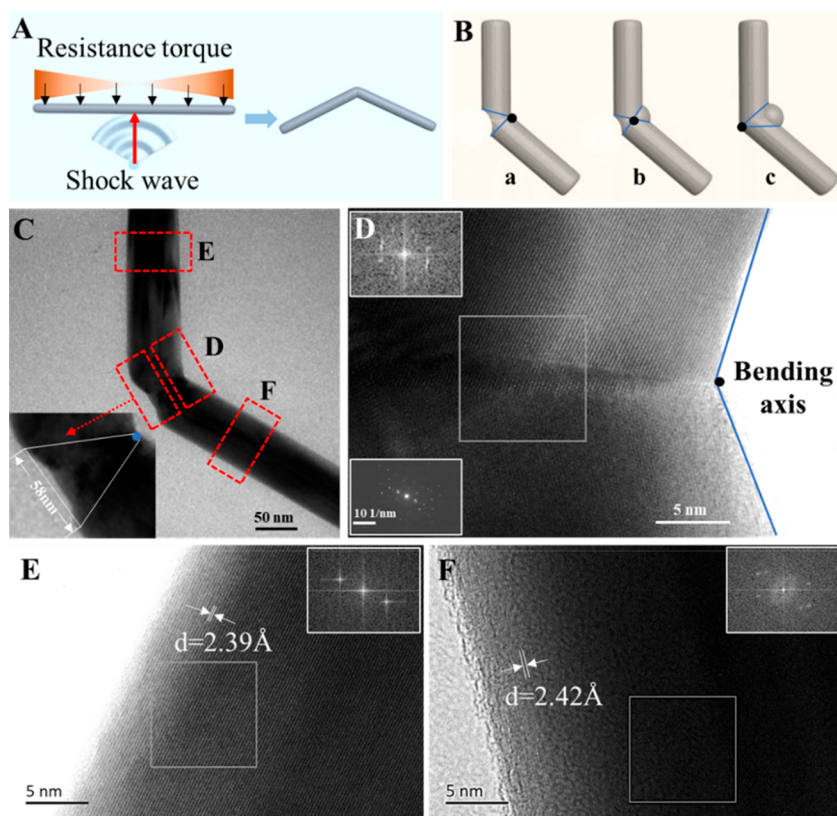


Figure 2. (A) Stress analysis of a bending Ag NW. (B) Schematics illustrating the effects of different bending axes. (C) TEM image of a typical bent Ag NW. (D–F) HRTEM and SAED diagrams of the corresponding positions in (C).

(Figure 1C), clearly proving that the Ag NWs were breaking. It is noteworthy that no smooth curving of Ag NW was observed. Each bending point is sharp and clean, as opposed to continuous gentle bends in macroscopic wires. This is likely because a gentle curving would be reversible and would quickly return the NW to the straight conformation.

Factors Affecting the Bending. Considering that ultrasonication increases the temperature of the entire water bath,

we carried control experiments to stir the Ag NWs at 60 °C for 24 h. The resulting Ag NWs were not bent (Figures S3 and S4), suggesting that the heating and weak shear stress are not the cause of the bending.

We speculate that both the Ag NW length and its distance from the cavitation are the critical factors of bending. As a shock wave propagates and makes contact with a Ag NW, it exerts an outward impact force on it. The impact force is

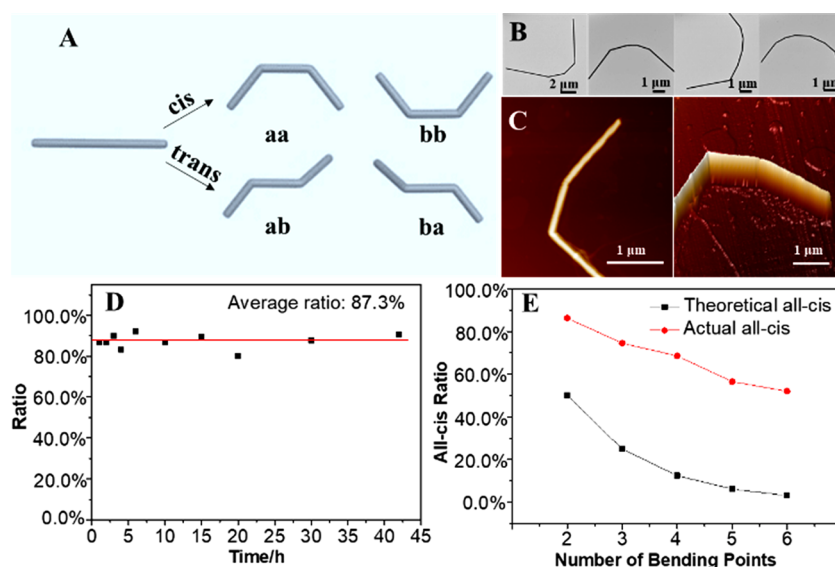


Figure 3. (A) The cis- and trans-conformations of the bent Ag NWs. (B) TEM images of the typical multi-segment bent Ag NWs. (C) Images of AFM representing cis-conformation is coplanar. (D) Temporal evolution of the percentage of the three-segment cis-bending. (E) The theoretical and actual percentages of all-cis multi-segment bent Ag NWs.

expected to be stronger near the initial impact point and weaker at the far ends. Meanwhile, the Ag NW is subjected to inertia and resistance in the opposite direction, the torque of which increases from the contact point to the two ends (Figure 2A). Thus, the imbalance of the two forces causes the Ag NW to bend. For a longer Ag NW, the force arms are longer, the torques are larger, and thus the Ag NW are more prone to bending (Figure 1E).

Ultrasound is a spherical wave, and thus its energy density is inversely proportional to R^2 :

$$I = \frac{P}{2\pi R^2} \quad (1)$$

In other words, a Ag NW closer to the cavity would experience higher energy density (Figure 1A) and is thus easier to bend (Figure 1E). In the experiment, the sample after 1 h sonication had a longer total length, a higher percentage of bending (89.3%), including many multi-segment structures; whereas the sample after 42 h sonication showed much shorter total length and a lower percentage of bending (51%), including mostly two- or three-segment structures. As shown in Figure 1C, the initial longer Ag NWs underwent a faster rate of breaking. The rate decreased as the length became shorter, along with the number of bends per Ag NW. As a longer Ag NW is susceptible to a shock wave of further distance, it would face a higher probability of bending. On the contrary, a shorter one would be more rigid, only responding to a shock wave at closer distance. Such dependence would explain the decreasing probability of breaking as the Ag NWs became shorter. The strong correlation between the two traces suggests that the breaking points occur at the existing bends, otherwise the trace of average bends would lag behind.

Bending Axis. Generally, when a wire is bent, the inner portion of the bend would experience compressive stress, whereas the outer portion experiences tensile stress (Figure 2A). As shown in Figure 2B, there are three possible scenarios: the bending axis may be inside, middle, and outside of the Ag NWs. When the bending axis is inside, it would open a “gap” on the outer portion of the bend, because geometrically the

outer rim is longer than the inner rim. As a metal, the Ag NW would rearrange its lattice to allow some Ag to “flow” and fill in the gap to help relax the stress. The process would create a concave surface as indicated in the diagram. When the bending axis is at the outer rim, the inner rim would have too many materials due to geometric constraints. The bending process would exclude the excess material as a bulge. Between the two extremes, when the bending axis is at the middle, the outer rim would form a small concave surface and the inner rim would form a small bulge. From this perspective, it is easy to understand why no bending occurs with an acute angle, because the gap would be too large to accommodate.

As shown in Figure 2C, the typical bend has no inner bulge, and the outer gap is about 58 nm, suggesting that the bending axis is near the inner side (Figure S10) and supporting the notion of an outward push by the shock wave. The straight segments of the Ag NW still maintained the original lattice structure, and only the newly torn gap experienced significant deformation. In the HRTEM images (Figure 2C–F and Figure S5), a clear twin plane is the most prominent and common feature. These phenomena are consistent with a clear-cut bending of simple crystalline structure, as opposed to polycrystalline macroscopic wires.^{17,18} An atomic simulation was carried out to understand the “flow” of Ag into the torn gap (Figure S15).¹⁹ The rearranged Ag atoms form a twin plane, suggesting that it is indeed a low-energy favorable state.

Interrelated Bending Events. For Ag NWs with three segments, there are two possible conformations: the cis- and trans-forms (Figure 3A). As shown in the AFM images (Figure 3C and Figure S12), the Ag NWs with cis-bending were coplanar. On the basis of two-dimensional TEM/SEM projection and assuming two independent bending events, the cis- and trans-forms would each account for 50% of the total (see detailed analysis in Table S1). In contrast, it was found that 87.3% of the three-segment Ag NWs are of the cis-conformation, and the ratio does not fluctuate with time (Figure 3D). Hence, the two bending events are not random but interdependent. As a shock wave could come from any direction, the result provides strong support that the multiple

bends are caused by a single action of a shock wave. More importantly, the multi-segment bent Ag NWs showed a high percentage of the cis-bending. With more bending points, the probability of the theoretical all-cis conformation would decrease exponentially (Figure 3B,E and Figure S8). Thus, the abnormal high percentage of cis-bending shows that the multiple bending events of each Ag NW are highly correlated, probably as part of a single event.

To investigate the correlation between the bending angle and length, we studied the statistics of the length ratio (L_1/L_2 , where L_1 is the shorter arm) and the angle ratio ($\angle 1/\angle 2$) of the three-segment cis-bending Ag NWs (Figure 4C). The

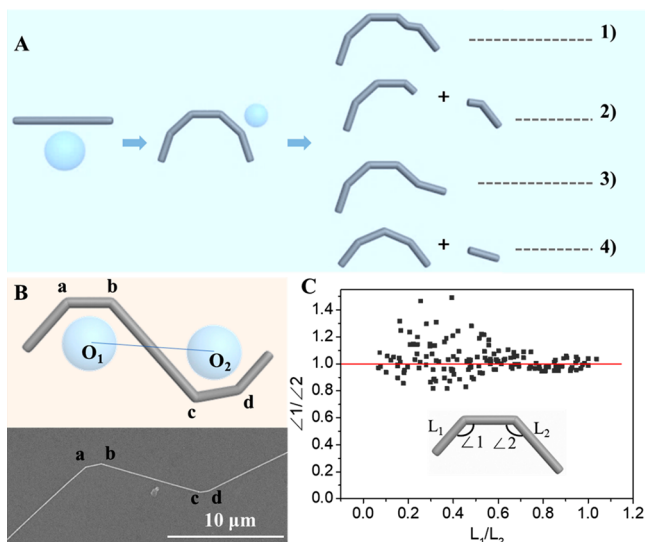


Figure 4. (A) Schematics illustrating the four possible scenarios of secondary bending and breaking. (B) Schematics and SEM image of multiple bends for a long Ag NW. (C) Dependence of length ratio and angle ratio of the three-segment cis-bending Ag NWs, where the shorter arm is named L_1 , the longer arm is L_2 , and their corresponding angles are $\angle 1$ and $\angle 2$.

result shows that the angle ratio fluctuates around 1, whereas the length ratio distributes broadly between 0.06 and 1. It is conceivable that a shock wave would act on any point on the Ag NW. For the Ag NWs with a L_1/L_2 ratio close to 1, their bending angles are also approximately equal, distributing at the vicinity of the red line. As similar arm length would experience similar resistance and torque, it is reasonable to expect similar bending angles. For the Ag NWs with a different arm length, the shock wave was probably off-center. The bending angles distributed more broadly, with roughly the same number of cases above and below the red line. The longer the arm, the larger the torque, the more extensive the bending, and thus, the smaller the bending angle, explaining the cases above the red line (Figure S2). However, the cases at the lower left corner do not conform to the analysis. We speculate that it may be due to the secondary bending of the Ag NWs.

The fact that the Ag NWs were broken after extensive sonication clearly suggests that multiple bendings were occurring to each Ag NWs. The questions are (1) whether the second bending occurs at a new site or at the same bending site of the first round; and (2) how many bendings could occur at a site before the Ag NW is broken. The exhaustive combination of the two aspects gives four possible scenarios (Figure 4A): (1) The second bending always occurs at a new

site, and the Ag NW is not easily broken. This would lead to an increase of the bending points per Ag NW, at least in the early stages, contradicting with Figure 1D. (2) The second bending leads to breaking at a new site. This is unlikely since the first round of bending clearly does not cause extensive breaking. The new site should be similar to the initial Ag NW in the tendencies of bending and breaking. (3) The second bending always occurs at an existing site, but the Ag NW is not easily broken. The Ag NWs would be bent multiple times under ultrasound at the same bending point. As the bending direction is random, it would lead to a large number of trans-conformations, contradicting with the majority of cis-conformations as shown in Figure 3E. (4) The second bending always occurs at an existing site causing breaking of the Ag NW. This would lead to 100% cis-conformations. Meanwhile, the rapid breaking of the Ag NW would coincide with the decrease of total length, as shown in Figure 1C. On these bases, we believe that the real scenario should be close to the scenario 4, where most of the cis-conformations (e.g., 87% of three-segment Ag NWs) are generated by the first bending event. The remaining few cases are caused by either bending at a new site or bending at an existing site without breaking.

An exception is when the two bending events are far from each other, giving relatively independent features. In our results, there are a number of structures containing two half-circular bends with opposite bending directions (Figure 4B). Careful analysis shows that the middle arm (bc) is always very long, suggesting that the cavities are independent with little mutual interference. Such a structure is rare (< 1%), indicating its low probability of formation. While cavities form randomly in the solution, those secondary cavities occurring near the first one have already been discussed (Figure 4A). In other words, the results would be recognizable only when the Ag NW is very long and when the second bending occurs far away from the first bending site.

Effective Radius of the Shock Wave. Among the thousands of bent Ag NWs we have surveyed, the overall shape never exceeds a semicircle. This phenomenon is consistent with the imbalance between the outward push by the shock wave and the opposite torque of inertia and fluid resistance. As such, the semicircle serves as an excellent indicator for the effective radius of the shock wave, which is otherwise extremely difficult to measure.

For any bent Ag NW, we tried to fit a circle inside, making tangent contacts with a maximum number of arms. The radius of such circle is defined as the effective radius of the shock wave. As such, simply breaking the multi-segment bends would not affect the effective radius, and only further bending events would be able to. Figure 5 shows the temporal evolution of the effective radius ($5\text{--}2\ \mu\text{m}$), along with the total length of the Ag NWs. As the Ag NWs become shorter, the average effective radius decreases, showing a strong correlation (Figure 5B). The distribution of the effective radius also became narrower. Its upper limit essentially means the farthest possible cavitation. The obvious decrease of the upper limit is consistent with the previous argument that a shorter Ag NW requires a cavity of closer proximity. In comparison, the decrease of the lower limit is less obvious. The closer cavity would generate a smaller torque, and thus a shock wave would pass it before a sufficiently large force could be exerted, leaving it unaffected.

In the literature, cavitation has been observed using laser light diffraction,²⁰ active cavitation detection,²¹ phase-

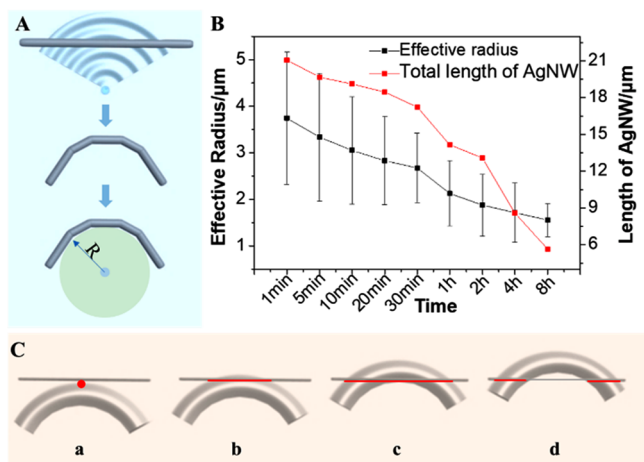


Figure 5. (A) Using multi-segment cis-conformations to define the effective radius of shock wave. (B) Temporal evolution of effective radius and total length. (C) Schematics illustrating the changes of the contact area as the shock wave passes through the Ag NW.

Doppler,²² and high-speed photography and holography,²³ where the minimal size of cavities is around $10\ \mu\text{m}$. Viewing smaller cavities, especially those in the earlier stages of development, remains a challenge. Moreover, the existing methods are suited for single cavity observation (stable cavitation), whereas multiple cavities (transient cavitation) will aggregate and interfere with each other.²⁴ Most importantly, the observation of a shock wave and its effect are so far impossible. From these perspectives, our system provides a perspective for understanding cavitation effects.

The reason cavitation generates a shock wave is that its collapse causes the surrounding liquid to rush towards its center. This implosion then rebounds to create a shock wave, with most of the energy focusing on the first wave. Figure 5C shows the first shock wave generated by the cavity, making an initial point of contact and then gradually passing through the Ag NW, assuming a rigid NW. At the initial point of contact, the shock wave would have the highest energy density, but the contact area is almost zero; as the contact area increases, the energy density would slightly decrease; and after the shock wave passes the Ag NW at the initial point, the contact area would move towards the ends, with decreasing contact area and energy density. Hence, it is clear that the impact force would first increase and then decrease. In reality, the Ag NW would certainly bend as the impact force pushes it outwards and the torque depends on the arm length from the point of contact. These analyses would explain the distribution of angle ratio ($\angle 1/\angle 2$) around 1 in Figure 4C, and that the longer arm tends to be bent further (smaller $\angle 2$). That is also why the bent NWs never exceed a half circle.

Moreover, as the Ag NWs broke during the sonication, the shorter NWs would become more rigid due to the shorter arm length and smaller torque. Thus, a longer NW would be bent by a cavity farther away: Even when the shock wave passes through a significant portion of the NW, the remaining arms outside the contact point still have a sufficient length to create enough torque. This would explain the larger effective radius for the longer NWs (Figure 5B). On the other hand, a shorter NW can only be bent by a cavitation nearby, and thus the effective radius is smaller. This would also explain the larger number of bends for longer NWs (Figure 3B) and, in

particular, the decrease of number of bends during sonication (Figure 1C).

Our surveys show that the sonication typically causes 2–4 segments at the middle of long nanowires. Even when the nanowire has excessive length, the remaining length will be in the long straight segments at the ends, as opposed to equal distribution of length among the segments. Hence, the fact that the bending events mostly occur near the contact point supports the decay of impact force as the shock wave passes the Ag NW. If the second shock wave has a similar strength as the first one, then we would expect it to further bend the nanowire beyond a semicircle. Thus, the absence of such structure is consistent with the argument of single shock wave, which also agrees with the macroscopic shock waves.

CONCLUSION

In summary, we used Ag NW as the model to study the mechanical effects of ultrasound on nanomaterials. The processes are clearly not random: (1) The bending axis is always near the inner surface of the bend (Figure 2B), tearing apart the outer portion and creating a twin plane; (2) the bending direction in multi-segment bends are mostly correlated, likely a part of the same bending event, that is, during the same shock wave; (3) the bending angles are correlated with the respective arm length, supporting our hypothesis of torque-induced bending; and (4) the effective radius of the shock wave is around $2\text{--}5\ \mu\text{m}$, which decreases with the total length of the Ag NWs.

While our initial study cannot be all-inclusive, we believe that it will help to exploit the mechanical effects of sonication for sophisticated nanosynthesis, for example, in multi-component systems and with multi-step manipulation. The collective structural analysis provides an alternative perspective for the field of nanomanipulation, in terms of revealing the mechanical properties of freely suspended colloidal nanostructures. Our work also highlights the significance of the morphological effects of sonication, which is often neglected and should be of broad interest considering the wide-spread use of sonication.

MATERIALS AND METHODS

Materials. All chemical reagents were used as purchased without further purification. Silver nitrate (AgNO_3 , 99.0%) and iron chloride hexahydrate ($\text{FeCl}_3 \cdot 6\text{H}_2\text{O}$, 98%) were purchased from Sigma-Aldrich. Poly(vinylpyrrolidone) ($\text{C}_6\text{H}_9\text{NO}$)_n (PVP, $M_w \sim 1,300,000$) was purchased from Alfa Aesar. Ethylene glycol ($\text{C}_2\text{H}_6\text{O}_2$, AR) and ethanol ($\text{C}_2\text{H}_5\text{O}$, AR) were purchased from Sinopharm Chemical Reagent Co., Ltd. Acetone ($\text{C}_3\text{H}_8\text{O}$, 99.5%) was purchased from Shanghai Lingfeng Chemical Reagent Co., Ltd.

Instruments. TEM images were collected from a Talos L120C model transmission electron microscope operated at 120 kV. Field emission scanning electron microscope (SEM) images were collected on a FEI Quanta 250 FEG model. Ultrasound machine is the KH-250DE type CNC ultrasonic cleaner operated at 250 W and 40 kHz.

Synthesis of Ag NWs. 0.300 g of PVP and 0.200 g of AgNO_3 were dissolved in 50 mL of ethylene glycol. A small amount of $\text{FeCl}_3 \cdot 6\text{H}_2\text{O}$ (0.100 mg, $12.5\ \mu\text{M}$) was added, and the mixture was stirred at room temperature until it was fully dissolved. Then, the solution was transferred to an oil bath and reacted at $130\ ^\circ\text{C}$ and 800 rpm for 8 h.

The as-synthesized Ag NWs were cleaned twice with acetone: First, 5 mL of acetone was added to 1 mL of the as-synthesized Ag NW solution, and the mixture was shook up and down, let stand, and removed of the supernatant. Then, 3 mL of acetone was added to the Ag NWs again, and the mixture was shook up and down, let stand,

and removed of the supernatant. Finally, the obtained Ag NWs were dispersed in ethanol and used as a stock solution.

Ultrasonic Treatment of Ag NWs. The purified Ag NWs were dispersed in ethanol (1 mg/mL). 1 mL of sample was put in a 4 mL glass bottle, which was placed on the action point of the ultrasonic cleaner and sonicated for 42 h. The liquid level in the glass bottle was kept as low as possible, so that the sample of Ag NWs was more uniformly affected during the ultrasonication. When ultrasonication was performed for 1 min, 3 min, 5 min, 10 min, 20 min, 30 min, 1 h, 2 h, 3 h, 4 h, 6 h, 10 h, 20 h, 30 h, and 42 h, aliquots of the samples were taken for characterization.

ASSOCIATED CONTENT

Supporting Information

The Supporting Information is available free of charge at <https://pubs.acs.org/doi/10.1021/acsnano.0c05601>.

Details of the synthesis and measurements; Figures S1–S15 and Table S1 with detailed discussions; SEM, TEM, AFM images, bending diagram, and statistical data diagram (PDF)

AUTHOR INFORMATION

Corresponding Authors

Hongyu Chen – Institute of Advanced Synthesis (IAS) and School of Chemistry and Molecular Engineering, Jiangsu National Synergetic Innovation Centre for Advanced Materials, Nanjing Tech University, Nanjing 211816, P.R. China; orcid.org/0000-0002-5325-9249; Email: iasychen@njtech.edu.cn

Xueyang Liu – Institute of Advanced Synthesis (IAS) and School of Chemistry and Molecular Engineering, Jiangsu National Synergetic Innovation Centre for Advanced Materials, Nanjing Tech University, Nanjing 211816, P.R. China; Email: ias_xyliu@njtech.edu.cn

Authors

Qiuxian Chen – Institute of Advanced Synthesis (IAS) and School of Chemistry and Molecular Engineering, Jiangsu National Synergetic Innovation Centre for Advanced Materials, Nanjing Tech University, Nanjing 211816, P.R. China

Wenwen Xin – Institute of Advanced Synthesis (IAS) and School of Chemistry and Molecular Engineering, Jiangsu National Synergetic Innovation Centre for Advanced Materials, Nanjing Tech University, Nanjing 211816, P.R. China

Qiaozhen Ji – Institute of Advanced Synthesis (IAS) and School of Chemistry and Molecular Engineering, Jiangsu National Synergetic Innovation Centre for Advanced Materials, Nanjing Tech University, Nanjing 211816, P.R. China

Ting Hu – Institute of Advanced Synthesis (IAS) and School of Chemistry and Molecular Engineering, Jiangsu National Synergetic Innovation Centre for Advanced Materials, Nanjing Tech University, Nanjing 211816, P.R. China

Jun Zhang – Key Laboratory of Unsteady Aerodynamics and Flow Control, Ministry of Industry and Information Technology, College of Aerospace Engineering, Nanjing University of Aeronautics and Astronautics, Nanjing 210016, P.R. China

Cheng Shang – Collaborative Innovation Center of Chemistry for Energy Material, Shanghai Key Laboratory of Molecular Catalysis and Innovative Materials, Key Laboratory of Computational Physical Science, Department of Chemistry,

Fudan University, Shanghai 200433, P.R. China;

orcid.org/0000-0001-7486-1514

Zhipan Liu – Collaborative Innovation Center of Chemistry for Energy Material, Shanghai Key Laboratory of Molecular Catalysis and Innovative Materials, Key Laboratory of Computational Physical Science, Department of Chemistry, Fudan University, Shanghai 200433, P.R. China;

orcid.org/0000-0002-2906-5217

Complete contact information is available at:

<https://pubs.acs.org/doi/10.1021/acsnano.0c05601>

Author Contributions

X.L. and H.C. designed and supervised the project. Q.C. and W.X. were responsible for most of the experiments and statistical analysis. Q.C., H.C., and X.L. worked on the mechanistic analyses and interpretations. Q.J. and T.H. provided help in SEM, TEM, and HRTEM characterization. J.Z. provided advice on the principle of acoustic cavitation. C.S. and Z.L. performed the atomic simulation. All authors participated in the writing of the manuscript.

Notes

The authors declare no competing financial interest.

ACKNOWLEDGMENTS

This work was supported by the National Natural Science Foundation of China (91956109 and 21673117), Youth Fund of Science and Technology Project of Jiangsu Provincial Department of Science and Technology (BK20180691), and Provincial Foundation for Specially-Appointed Professor, startup fund at Nanjing Tech University (38274017110 and 39837102).

REFERENCES

- (1) Suslick, K. S. Sonochemistry. *Science* **1990**, *247*, 1439–1445.
- (2) Jiang, L.-P.; Xu, S.; Zhu, J.-M.; Zhang, J.-R.; Zhu, J.-J.; Chen, H.-Y. Ultrasonic-Assisted Synthesis of Monodisperse Single-Crystalline Silver Nanoplates and Gold Nanorings. *Inorg. Chem.* **2004**, *43*, 5877–5883.
- (3) Li, H.; Zhang, P.; Smaga, L. P.; Hoffman, R. A.; Chan, J. Photoacoustic Probes for Ratiometric Imaging of Copper(II). *J. Am. Chem. Soc.* **2015**, *137*, 15628–31.
- (4) Hertzberg, Y.; Volovick, A.; Zur, Y.; Medan, Y.; Vitek, S.; Navon, G. Ultrasound Focusing Using Magnetic Resonance Acoustic Radiation Force Imaging: Application to Ultrasound Transcranial Therapy. *Med. Phys.* **2010**, *37*, 2934–42.
- (5) Sato, K.; Li, J.-G.; Kamiya, H.; Ishigaki, T. Ultrasonic Dispersion of TiO₂ Nanoparticles in Aqueous Suspension. *J. Am. Ceram. Soc.* **2008**, *91*, 2481–2487.
- (6) Furusawa, Y.; Fujiwara, Y.; Campbell, P.; Zhao, Q. L.; Ogawa, R.; Hassan, M. A.; Tabuchi, Y.; Takasaki, I.; Takahashi, A.; Kondo, T. DNA Double-Strand Breaks Induced by Cavitation Mechanical Effects of Ultrasound in Cancer Cell Lines. *PLoS One* **2012**, *7*, No. e29012.
- (7) Miller, D. L.; Thomas, R. M.; Buschbom, R. L. Comet Assay Reveals DNA Strand Breaks Induced by Ultrasonic Cavitation *in Vitro*. *Ultrasound in Med. & Biol.* **1995**, *21*, 841–848.
- (8) Xu, H.; Zeiger, B. W.; Suslick, K. S. Sonochemical Synthesis of Nanomaterials. *Chem. Soc. Rev.* **2013**, *42*, 2555–67.
- (9) Shchukin, D. G.; Mohwald, H. Sonochemical Nanosynthesis at the Engineered Interface of a Cavitation Microbubble. *Phys. Chem. Chem. Phys.* **2006**, *8*, 3496–506.
- (10) Kubota, R.; Yamashita, Y.; Kenmotsu, T.; Yoshikawa, Y.; Yoshida, K.; Watanabe, Y.; Imanaka, T.; Yoshikawa, K. Double-Strand Breaks in Genome-Sized DNA Caused by Ultrasound. *ChemPhysChem* **2017**, *18*, 959–964.

- (11) Bang, J. H.; Suslick, K. S. Applications of Ultrasound to the Synthesis of Nanostructured Materials. *Adv. Mater.* **2010**, *22*, 1039–59.
- (12) Mdleleni, M. M.; Hyeon, T.; Suslick, K. S. Sonochemical Synthesis of Nanostructured Molybdenum Sulfide. *J. Am. Chem. Soc.* **1998**, *120*, 6189–6190.
- (13) Mayers, B. T.; Liu, K.; Sunderland, D.; Xia, Y. Sonochemical Synthesis of Trigonal Selenium Nanowires. *Chem. Mater.* **2003**, *15*, 3852–3858.
- (14) Caneba, G. T.; Dutta, C.; Agrawal, V.; Rao, M. Novel Ultrasonic Dispersion of Carbon Nanotubes. *J. Miner. Mater. Charact. Eng.* **2010**, *09*, 165–181.
- (15) Retamal Marín, R. R.; Babick, F.; Stintz, M. Ultrasonic Dispersion of Nanostructured Materials with Probe Sonication – Practical Aspects of Sample Preparation. *Powder Technol.* **2017**, *318*, 451–458.
- (16) Zhang, Y.; Guo, J.; Xu, D.; Sun, Y.; Yan, F. One-Pot Synthesis and Purification of Ultralong Silver Nanowires for Flexible Transparent Conductive Electrodes. *ACS Appl. Mater. Interfaces* **2017**, *9*, 25465–25473.
- (17) Zhang, F.; Zhou, J. Tension-Compression Asymmetry and Twin Boundaries Spacings Effects in Polycrystalline Ni Nanowires. *J. Appl. Phys.* **2016**, *120*, No. 044303.
- (18) Park, H. S.; Cai, W.; Espinosa, H. D.; Huang, H. Mechanics of Crystalline Nanowires. *MRS Bull.* **2009**, *34*, 178–183.
- (19) Wang, C.; Wei, Y.; Jiang, H.; Sun, S. Bending Nanowire Growth in Solution by Mechanical Disturbance. *Nano Lett.* **2010**, *10*, 2121–5.
- (20) Burdin, F.; Tsochatzidis, N. A.; Guiraud, P.; Wilhelm, A. M.; Delmas, H. Characterisation of the Acoustic Cavitation Cloud by Two Laser Techniques. *Ultrason. Sonochem.* **1999**, *6*, 43–51.
- (21) Chen, W.-S.; Matula, T. J.; Crum, L. A. The Disappearance of Ultrasound Contrast Bubbles: Observations of Bubble Dissolution and Cavitation Nucleation. *Ultrasound in Med. & Biol.* **2002**, *28*, 793–803.
- (22) Tsochatzidis, N. A.; Guiraud, P.; Wilhelm, A. M.; Delmas, H. Determination of Velocity, Size and Concentration of Ultrasonic Cavitation Bubbles by the Phase-Doppler Technique. *Chem. Eng. Sci.* **2001**, *56*, 1831–1840.
- (23) Lauterborn, W.; Hentschel, W. Cavitation Bubble Dynamics Studied by High Speed Photography and Holography. *Ultrasonics* **1985**, *23*, 260–268.
- (24) Ashokkumar, M. The Characterization of Acoustic Cavitation Bubbles - An Overview. *Ultrason. Sonochem.* **2011**, *18*, 864–72.